Processing and Application of Ceramics 12 [1] (2018) 36–44
https://doi.org/10.2298/PAC1801036S

Structure and dielectric behaviour of Sr-modified $Bi_4Si_3O_{12}$ thin films prepared via sol gel method

Abbas Sadeghzadeh-Attar*, Saeid Hajijafari-Bidgoli, Mohammad Reza Bafandeh

Department of Metallurgy and Materials Engineering, University of Kashan, P.O. Box. 87317-53153, Ghotb Ravandi Blvd., Kashan, Iran

Received 8 October 2017; Received in revised form 21 November 2017; Accepted 3 February 2018

Abstract

Bismuth silicate ($Bi_4Si_3O_{12}$, BSO) nanostructured films containing 0, 1, 2, and 3 mol% Sr were prepared via sol-gel method and annealed at different temperatures up to 700 °C. The effects of Sr content on the structure and morphology of prepared films were investigated. SEM images showed that surfaces of the prepared films were dense, smooth and homogeneous. The average particle size was changed from 30 to 35 nm as the annealing temperature was increased from 500 to 700 °C. Variation of the dielectric constant and dielectric loss as a function of frequency and annealing temperature for the synthesized thin films with different content of Sr were also studied. The dielectric constant and dielectric loss decrease with Sr addition, and reach the minimum for the sample containing 2 mol% Sr. These changes could be attributed to the crystal structure and formation of secondary phases.

Keywords: *Sr-doped $Bi_4Si_3O_{12}$, thin films, sol-gel process, structural characterization, dielectric properties*

I. Introduction

In recent decades, ferroelectric thin films have attracted much attention due to their potential applications in sensors, capacitors, micro electro-mechanical system (MEMS), nonvolatile ferroelectric random access memory, and electro-optical devices [1–3]. Among related materials of interest, bismuth silicate ceramics with the layered perovskite structure are the most promising candidates for optical devices, optical laser and ferroelectric memories because of their low dielectric permittivity, high Curie temperature, high remanent polarization, optical activity, photoconductivity and photorefractive properties, and relatively low toxicity [4–8]. The layered compounds were studied for the first time by Aurivillius [9], who discovered a new phase with layered structure in the Bi_2O_3-TiO_2 system. He described the structure as formed by bismuth oxide based layers interleaved with pseudo-perovskite-type layers.

In the Bi_2O_3-SiO_2 system there is a large number of crystalline ternary bismuth compounds, such as Bi_2SiO_5, $Bi_4Si_3O_{12}$ and $Bi_{12}SiO_{20}$ [10–14]. One of the most common compounds in the Aurivillius family is $Bi_4Si_3O_{12}$ (BSO) similar to $Bi_4Ti_3O_{12}$ that could be presented by the general formula $[Bi_2O_2][A_{n-1}(B)_nO_{3n+1}]$. This compound consists of fluorite-like $(Bi_2O_2)^{2+}$ units alternating with perovskite-like $[A_{n-1}(B)_nO_{3n+1}]^{2-}$ blocks [15–20]. In the Aurivillius formula, A is a mono-, di- or tri-valent large cation in 12-fold cation sites which can be occupied by Ba^{2+}, Ca^{2+}, Bi^{3+} and the rare earth cations, while B is a tri-, tetra-, penta- or hexa-valent small cation such as Ti^{4+}, Nb^{5+} and W^{6+} [15–17]. Either A-site or B-site substitution can improve dielectric and ferroelectric properties of BSO, but the mechanism is different for each substitute. For A-site substitution, there is a highly asymmetric double-well potential at BO_6 octahedra unit adjacent to the interleaving Bi_2O_2 layer along the *c*-axis, and it results in the development of remanent polarization along the *c*-axis. For B-site substitution, the decrease in *c*-axis orientation results in the development of remanent polarization. For further improvement of ferroelectric properties, A and B-site substitution by various ions should be considered because the properties of BSO based materials depend strongly on species of the substituent ions [20–27].

In the general formula $[Bi_2O_2][A_{n-1}(B)_nO_{3n+1}]$ *n* is an integer named integration factor (the number of BO_6 oc-

* Corresponding author: tel: +98 031 55912492,
e-mail: *sadeghzadeh@kashanu.ac.ir*

tahedra in each pseudo perovskite block and can be n = 1–5). The compounds with an odd number of perovskite layers crystallize in *B*2*cb*, while even-layered members prefer *A*21*am* system. Thus, if n is even, the centre of the pseudo-perovskite set of layers is the A position and there is a mirror plane normal to c-axis. On the other hand, if n is odd the centre is in B position and the mirror plane divides the octahedrons. The parallel plane to $[Bi_2O_2]^{2+}$ layers is defined as the *ab* plane of unit cell, so the piling up of layers occurs along the c-axis [20].

$Bi_4Si_3O_{12}$ ceramics are the most important scintillation materials which are widely used in high energy physics, nuclear medical imaging and computer tomography due to their good mechanical, chemical, electro-optical and the thermoluminescence properties [28,29]. Several attempts to synthesize bismuth silicate thin films have been reported via chemical vapour deposition (CVD) [30], sol-gel [10,31] and pulse laser deposition methods [32,33]. Synthesis at low temperature, possibility for fabrication of complex and homogeneous compounds, low cost and environmentally friendly are the advantages of sol-gel method, so it has attracted the attention of many researchers in order to synthesize ceramic powders as well as thin films [34]. This method makes it possible to obtain doped films, which permit varying their physical properties (electrical conductivity, photoconductivity, optical absorption spectra, and others) purposefully. The main obstacle to use the sol-gel method is the complexity of the chemical process, due to the multicomponent nature of the composition [35]. However, the most important advantage of sol-gel over conventional coating methods is the ability to tailor the microstructure of the deposited films [36].

The aim of the present work is investigation of the effect of strontium addition on the structure, appearance of secondary phases, microstructure and the dielectric behaviour of nanostructure bismuth silicate thin films in order to improve the piezoelectric properties.

II. Materials and methods

Bismuth silicate ($Bi_4Si_3O_{12}$; BSO) thin film was prepared by sol-gel method using bismuth nitrate pentahydrate ($Bi(NO)_3{\times}5\,H_2O$) and tetraethyl orthosilicate (TEOS; $Si(OC_2H_5)_4$) as starting materials. Ethanol was used as solvent, whereas glacial acetic acid was used simultaneously as solvent and catalyst. All chemicals used were analytical reagents.

In order to prepare stable and homogeneous precursors, it was necessary to find the way to synthesize sols having stability over longer period. The main problem was that the bismuth precursor reacts easily with H_2O to yield white precipitate $BiONO_3$ and produces solution which is unstable and decomposes within a short time. Because of that the required amount of water for hydrolysis was supplied from water present in bismuth nitrate crystals. Thus, in a typical procedure transparent solution was formed by dissolving 1.21 g bismuth nitrate in 2 ml glacial acetic acid and 4 ml deionized water according to the relevant stoichiometric ratio (4 : 3). This solution was stirred for several minutes at room temperature. Subsequently, the mixture of 0.4 ml tetraethyl orthosilicate, 4 ml ethanol and 0.2 ml acetylacetone were slowly dropped into the above solution under a constant stirring rate. The proposed reactions for $Bi_4Si_3O_{12}$ phase formation are as follows [37]:

$$Si(OC_2H_5)_4 + 4\,H_2O \longrightarrow Si(OH)_4 + 4\,C_2H_5OH$$

$$3\,Si(OH)_4 + Bi(NO_3)_3 \longrightarrow Bi(OSi(OH)_3)_3 + 3\,HNO_3$$

Sr-solution was prepared by dissolving a specific amount of strontium acetate [$Sr(CH_3COO)_2$] into acetic acid and deionized water. Strontium-bismuth silicate sols, containing 1, 2 and 3 mol% Sr (denoted as BSS1, BSS2 and BSS3, respectively), were prepared by mixing the BSO- and Sr-solutions. The films were produced by dip-coating onto glass slide substrates with withdrawal speed of 1 mm/s. The coated films were dried for 1 h at 100 °C under ambient conditions, and further heated in the temperature range from 500–700 °C for 1 h in a muffle furnace to promote the crystallization of the samples. A general flow chart of all the steps used in the preparation of bismuth silicate and strontium-bismuth silicate thin films is illustrated in Fig. 1.

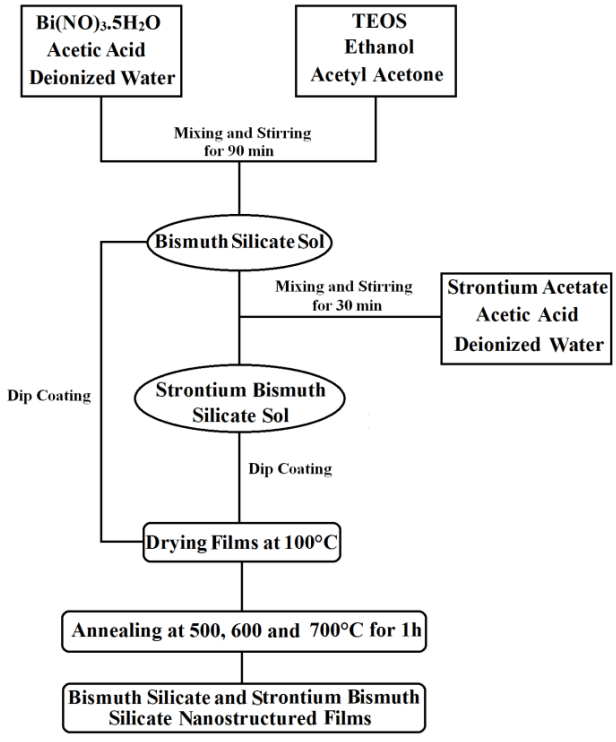

Figure 1. Flow chart for the fabrication of bismuth silicate and strontium-bismuth silicate thin films by sol-gel process

Thermal behaviour and phase transformation of the samples were examined by differential scanning calorimetry (DSC) and thermogravimetric analysis (TG) up to 800 °C on Netzsch STA 409 PC Luxx in air atmosphere at a heating rate of 10 °C/min. A mass spectrometer connected to the TG apparatus allows the

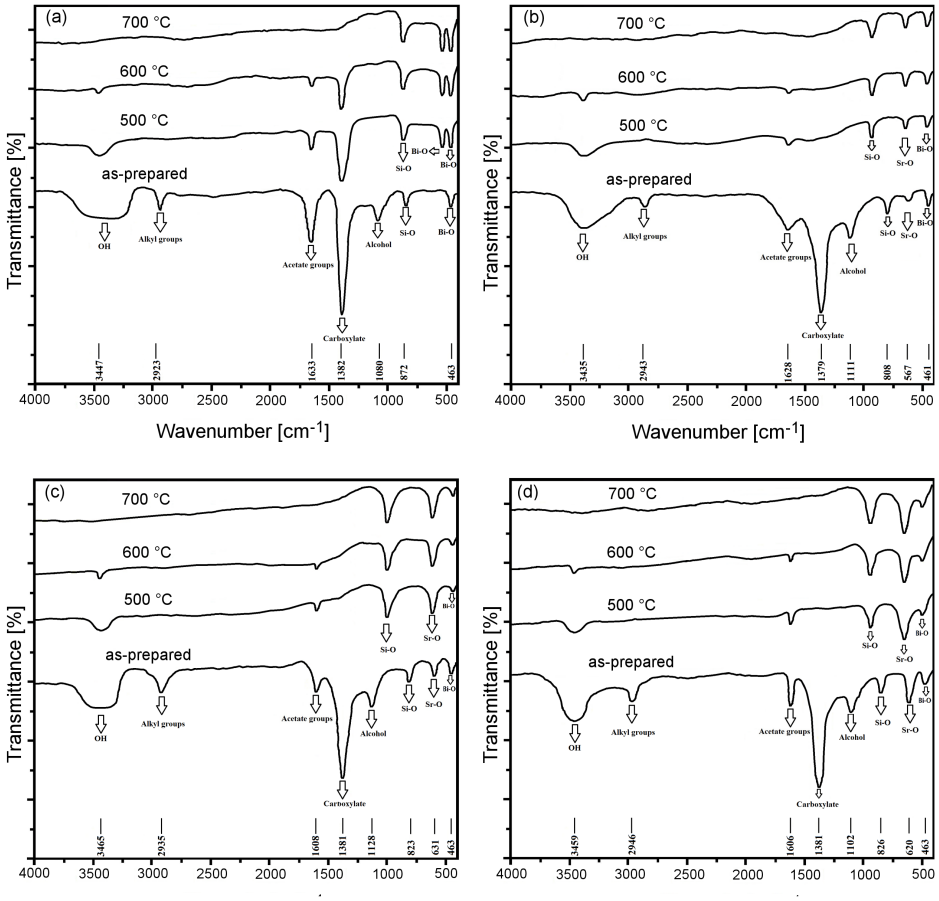

Figure 2. FT-IR spectra of as-synthesized thin films and annealed at 500, 600, and 700 °C for 1 h: a) BSO, b) BSS1, c) BSS2 and d) BSS3

identification of the released products during heating. Alumina was used as the reference material. Phase analysis was studied using X-ray diffraction method (XRD, X'pert PRO MRD, Philips) and CuK_α radiation. FT-IR measurements were recorded in transmission mode using Bruker TENSOR27 spectrophotometer, in the range between 400 and 4000 cm^{-1} with a resolution of 4 cm^{-1}. Structure of the prepared films was analysed by scanning electron microscopy (LEO 1450 VP Microscope operating at 15 kV). Dielectric constant and dielectric loss were measured using a LCR meter (model INSTEC LCR-821) at ambient temperature. Prior to the dielectric properties measurements, a thin layer of gold was sputtered as top and bottom electrodes through a mask onto the surface of thin films and substrate, respectively. Two ends of conductive electrode were connected with the LCR meter. The dielectric constant ε of the samples was calculated using values measured for the capacitance from 1 Hz to 10 MHz frequency range.

III. Results and discussion

The structure changes during the synthetic process were evaluated by FT-IR analysis. FT-IR spectra of the synthesized samples before and after annealing at different temperatures are presented in Fig. 2. From Fig. 2a (the pure bismuth silicate BSO sample) it can be seen that a broad peak appearing at 3200–3600 cm^{-1} as well as bands around 3394 and 1634 cm^{-1}, which are related to the stretching vibration of −OH groups, corresponding to the residual water and alcohol [37]. Intensities of these two peaks gradually decrease with the increase in annealing temperature. Absorption peak around 2923 cm^{-1} is due to the alkyl group bonds. This absorption peak is probably related to symmetric and antisymmetric stretching vibrations of methyl (CH_3) group [37]. In addition, with the increase in the annealing temperature, this peak disappeared at temperature higher than 500 °C. Peaks in the range 1550–1750 cm^{-1} are characteristic peaks of remained acetate and acetylacetone groups which are bound to surface sites of metal ions (such as Si). Reactions between TEOS and acetylacetone could be explained by presence of these bonds. Acetylacetone provides a strong bond with precursors and complex species [38]. Often the remained complex ligands are removed after heat treatment at temperatures higher than 700 °C. The chelation of metal ions resulted in the formation of metal carboxylate complexes, as observed from the symmetric and antisymmetric stretching vibrations of carboxyl (−COO) groups

at around 1382 cm^{-1} [38]. The intensity of the related peaks of acetate and carboxylate groups decreases after annealing at 500 and 600 °C and these peaks are completely removed after annealing at 700 °C (Fig. 2a). Moreover bonds in the range 1000–1200 cm^{-1} could be arising from alcoholic bonds in TEOS and ethanol groups. Therefore, the absorption at 1080 cm^{-1} may also be due to CH_3 rocking and CH_3–C–CH_3 stretching vibration modes. Generally absorptions below 1000 cm^{-1} are related to metal-oxygen bonds, i.e. Sr–O, Bi–O and Si–O. According to this, absorptions at 872 cm^{-1} and 463 cm^{-1} are related to Si–O and Bi–O bonds, respectively, and confirm formation of SiO_4 tetrahedral and Bi–O–Si bonds [39]. By comparing FT-IR spectra of the as-prepared and annealed BSO at different temperatures, it could be observed that the increase in annealing temperature up to 700 °C strongly reduces intensity of some peaks. On the other hand, the intensities of the Si–O, Sr–O and Bi–O peaks increase with the increase of annealing temperature indicating that the crystallinity increases with the annealing temperature [40], which is consistent with the XRD results. Absorption peaks at 478 and 534 cm^{-1} are assigned to Bi–O bonds which are more intense for the annealed BSO compared to the as-prepared BSO samples. Appearance of Si–O and Bi–O bonds indicates formation of SiO_4 tetrahedron and Bi–O–Si bonds [39]. When the hydrolysis reaction begins, Si–O–C vibration is substituted by Si–O(H) stretching vibration in 1000–1200 cm^{-1} range.

Figures 2b,c,d show FT-IR spectra of the Sr-bismuth silicate samples BSS1, BSS2, and BSS3. Since the only difference between these samples is in amount of Sr, their FT-IR spectra are similar to each other. Absorption peaks around 2943 cm^{-1} and 1628 cm^{-1} can be related to alkyl group bonds and acetylacetone groups connected to Bi, Si and Sr ions, respectively. Absorption peaks around 1379 cm^{-1} and 1083 cm^{-1} correspond to carboxylate bonds and CH_3 rocking as well as CH_3–C–CH_3 stretching vibrations, respectively [31]. Among peaks below 1000 cm^{-1}, those in the range 800–915 cm^{-1} are related to Si–O bonds and peaks around 480 cm^{-1} correspond to Bi–O bonds. Absorption peak around 621 cm^{-1} in FT-IR spectra of the BSS1, BSS2 and BSS3 samples, which is not seen in the BSO sample, is related to Sr–O bonds [41]. Thus, it could be concluded that increase in Sr content is accompanied with the increase in intensity of Sr–O peak and decrease in intensity of Bi–O peaks, while Si–O peaks remained nearly unchanged.

The TG and DSC results of the as-synthesized BSO and BSS2 samples are shown in Fig. 3. As shown in Fig. 3a, a large weight loss was observed in the temperature range between 100 and 140 °C. Besides, the DTA plot shows the presence of a sharp endothermic peak at approximately 90 °C. This corresponds to about 28.5% weight loss in TG curve due to the evaporation of the water and the organic solvent that caused heat absorption [42]. The exothermic peaks at approximately 295 and 418 °C, which corresponded with about 17.5% weight loss in TG curve, can be attributed to thermal decomposition of alkoxide bonds, residual organic materials and nitrate groups during combustion [42,43]. The second endothermic peak, located at about 700 °C corresponding to the third weight loss of about 2% in TG curve, is related to the crystallization of bismuth silicate and formation of perovskite structure [44]. At temperature higher than 700 °C no other weight changes in TG curve can be seen. These results are in good agreement with the XRD analysis of the samples annealed at different temperatures.

Similar results were obtained for the as-synthesized samples containing strontium. Figure 3b illustrates the TG-DTA curves of the as-synthesized BSS2 sample in the range of 20–800 °C. There are three pedestal sits of weight loss. The first one appears at about 70–120 °C corresponding to the main endothermic peak in DSC curve. Similar to the BSO sample, it is due to the evaporation of water and O–H groups. The second pedestal sit of weight loss appears in the range of 300–500 °C, and it is caused by the decomposition of alkoxides and nitrate groups and burning of residual organic materials. It can be seen (Fig. 3b) that by addition of Sr, intensities of two exothermic peaks in TG curve increase. The last pedestal sit of weight loss is located in the range of 680–700 °C. The DTA and TG indicated that this endothermic peak, due to the crystallization process and the secondary phases [40], is shifted to lower temperatures (690 °C) for the BSS2 sample. The intensity of this endothermic peak decreases with increase of Sr amount. On the other hand, different amounts of Sr do not have significant influence on the thermal behaviour of the fabricated thin films. The DSC curves suggested that the

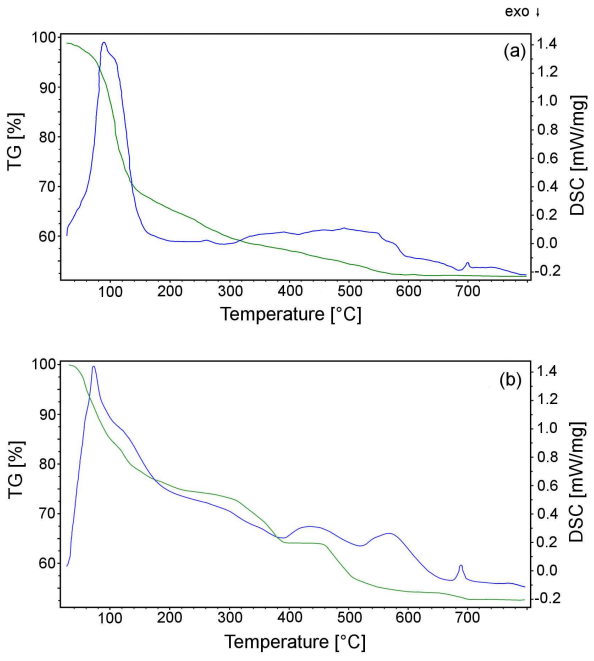

Figure 3. TG-DSC curves of the as-synthesized: a) BSO and b) BSS2 samples

annealing temperature of the as-synthesized thin films should be higher than 690 °C. Therefore, according to the results of thermal behaviour, the prepared films were annealed at 700 °C for 1 h.

XRD patterns of the prepared BSO films after annealing at 500, 600 and 700 °C for 1 h are shown in Fig. 4. The BSO sample annealed at 500 °C consists of SiO_2, Bi_2SiO_5 and $Bi_{12}SiO_{20}$ phases. The Bi_2SiO_5 is formed according to the following reaction [37,45]:

$$Bi_2O_3 + SiO_2 \longrightarrow Bi_2SiO_5 \quad (1)$$

By increasing annealing temperature, the peaks related to Bi_2SiO_5 phase disappeared. Moreover, the peaks related to SiO_2 become less intense and the peaks related to $Bi_{12}SiO_{20}$ are stronger. The following reactions could be expected [37]:

$$6Bi_2SiO_5 \longrightarrow Bi_{12}SiO_{20} + 5SiO_2 \quad (2)$$

$$Bi_{12}SiO_{20} + 8SiO_2 \longrightarrow Bi_4Si_3O_{12} \quad (3)$$

XRD results confirmed that the formation of $Bi_4Ti_3O_{12}$ phase started at 600 °C. It can be seen (Fig. 4) that with the increase in annealing temperature the width and intensity of XRD peaks decreased and increased, respectively. A single phase of $Bi_4Si_3O_{12}$ with perovskite structure was obtained without any secondary phase, after annealing at 700 °C. The observed peaks at $2\theta = 21.3, 27.5, 32.8, 35, 43.2, 45, 52$ and $55.1°$ are related to (211), (310), (321), (400), (422), (431), (530) and (532) planes, respectively [46].

Figure 5 shows XRD patterns of the BSS1, BSS2, and BSS3 samples annealed at 700 °C for 1 h. The presence of a secondary phase $Bi_6Sr_2O_{11}$, besides $Bi_4Si_3O_{12}$ as the main phase, is clearly seen in the sample BSS1. The presence of this secondary phase modifies the structure of the BSS1 film through a pinning effect exerted and as a consequence decreases grain size [47]. Secondary phases including $Sr_2Bi_2O_5$ and Sr_2Si_3 can be observed in XRD pattern of the BSS2 sample (Fig. 5). Other secondary phases such as $Sr_4Si_4O_{12}$ and $Sr_3Si_3O_9$ are present in the BSS3 sample annealed at 700 °C. The relative intensity of 211 peak decreases with the increase in the Sr amount. The bismuth silicate sample with higher Sr amount (BSS3) contains a large amount of secondary phase. Previous studies [48] have shown that the secondary phases can affect the optical properties of nanostructured strontium-bismuth silicate layers. The mean crystallite sizes of the annealed BSO, BSS1, BSS2 and BSS3 samples at 700 °C were calculated according to Scherrer equation [49], and estimated to be 22, 20, 15 and 18 nm, respectively. Therefore, the size of crystallites decreases with the increase in Sr contents. The grain boundaries are suitable sites for nucleation and the presence of doped element at grain boundaries can hinder grain growth [50].

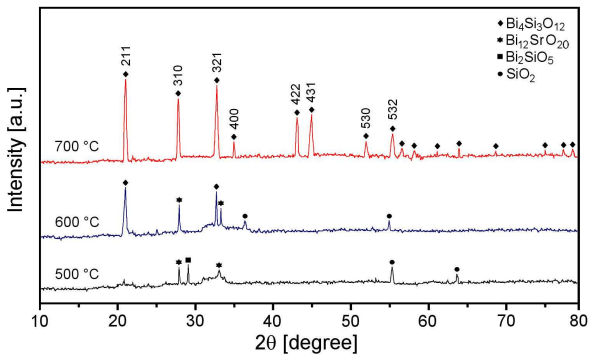

Figure 4. XRD patterns of the BSO nanostructured films annealed at different temperatures (a) 500, (b) 600, and (c) 700 °C for 1 h

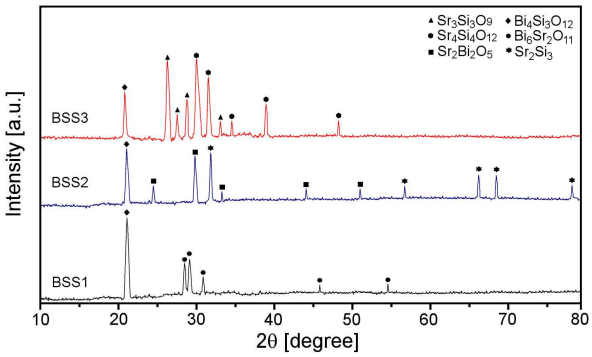

Figure 5. XRD patterns of the (a) BSS1, (b) BSS2, and (c) BSS3 nanostructured films annealed at 700 °C for 1 h

Figure 6 shows the SEM microstructure of the BSS2 films annealed at 500, 600 and 700 °C for 1 h. The surfaces of the films were smooth and dense with the particles which are almost spherical. These particles were evenly distributed, and their size becomes larger as the annealing temperature increases, so that the mean particle size is about 30, 32 and 35 nm for samples annealed at 500, 600 and 700 °C, respectively. According to SEM images, in some regions asymmetric agglomerated grains can be seen. This observation could be due to the nature of sol-gel process. Another factor which was responsible for agglomeration was annealing the samples at relatively high temperature for a long time, which enhanced diffusion and consequently, grain growth [51]. The cross-section of the nanostructured BSS2 film annealed at 700 °C for 1 h, shown in Fig. 6d, confirmed that thickness of the obtained film is about 180 nm.

Figure 7a shows dielectric constant as a function of applied frequency for different samples after annealing at 700 °C for 1 h. Decrease in dielectric constant due to the increase in frequency was observed [52]. It could also be concluded that addition of Sr up to 2 mol% results in the decrease in dielectric constant. Further addition of Sr was accompanied with increase in dielectric constant. This observation could be related to the finer grain structure of the sample BSS2 containing 2 mol% Sr and presence of secondary phases. It is well known that the dielectric constant of ceramics is sensitive to the morphology, crystal structure, phase composition, and the grain size [53–55]. Thus, smaller grain size due

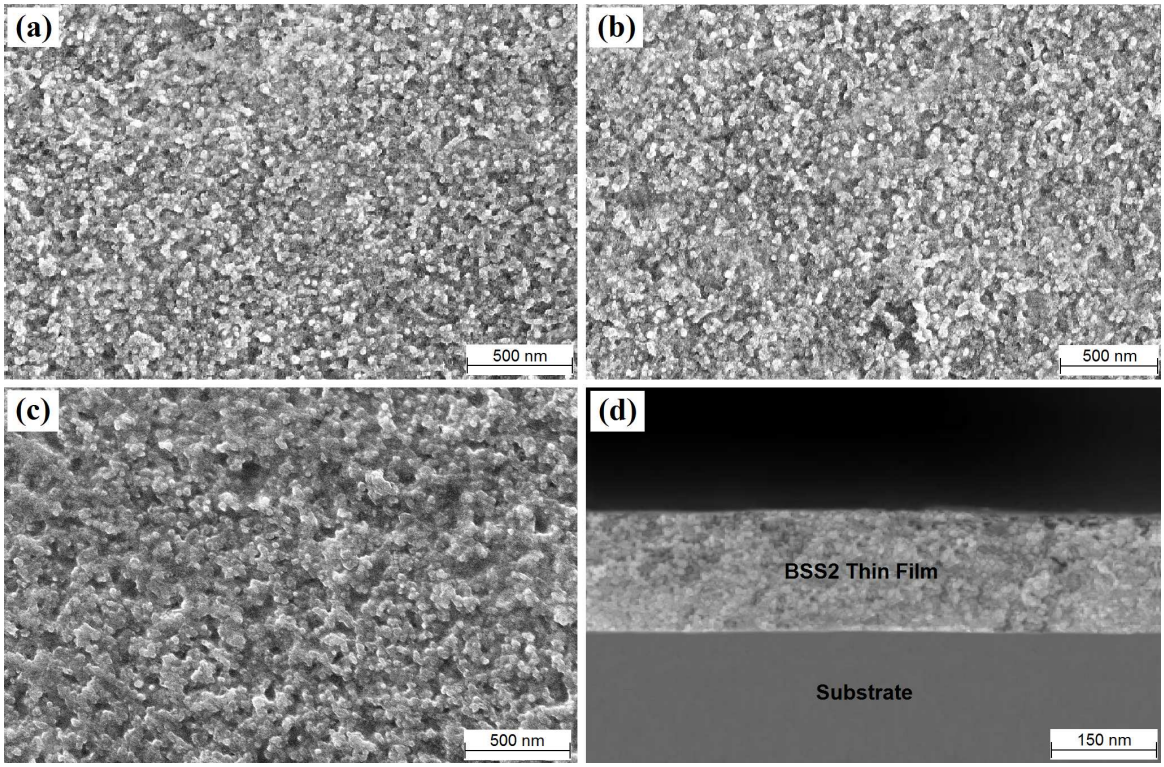

Figure 6. Microstructures of the BSS2 nanostructured films - surface structures of the film annealed at: a) 500, b) 600, c) 700 °C for 1 h, and d) cross-section of the film annealed at 700 °C for 1 h

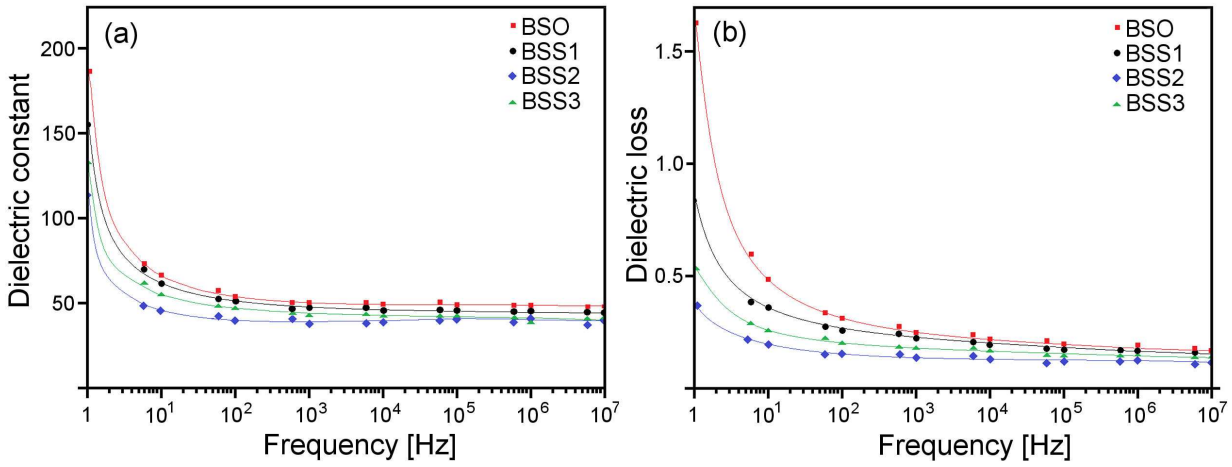

Figure 7. Variation of: a) dielectric constant and b) dielectric loss as a function of frequency for BSO, BSS1, BSS2, and BSS3 samples

to the presence of secondary phases usually results in lower polarization and, therefore, gives lower value of dielectric constant. In finer microstructure, the number of grain boundaries and the amount of internal stress increases, therefore, dipole rotation becomes more difficult and as a result polarization and dielectric constant decrease [56]. In addition, presence of Sr results in formation of secondary phases. Dielectric constant of these phases is lower than for $Bi_4Si_3O_{12}$ and therefore dielectric constant of the BSO film is higher than the films doped with Sr (Fig. 7a).

Figure 7b shows dielectric loss as a function of frequency for different samples after annealing at 700 °C for 1 h. Dielectric loss, as a measure of waste energy in dielectric material during electric field application, decreases with frequency. It can be also seen that dielectric loss first decreases with increasing Sr content (up to 2 mol%) and then increases. It is well known that dielectric loss is strongly dependent on microstructural factors, such as lattice defects (vacancies, dislocations, grain boundaries, and impurities), secondary phases, porosity, crystallinity and other processing re-

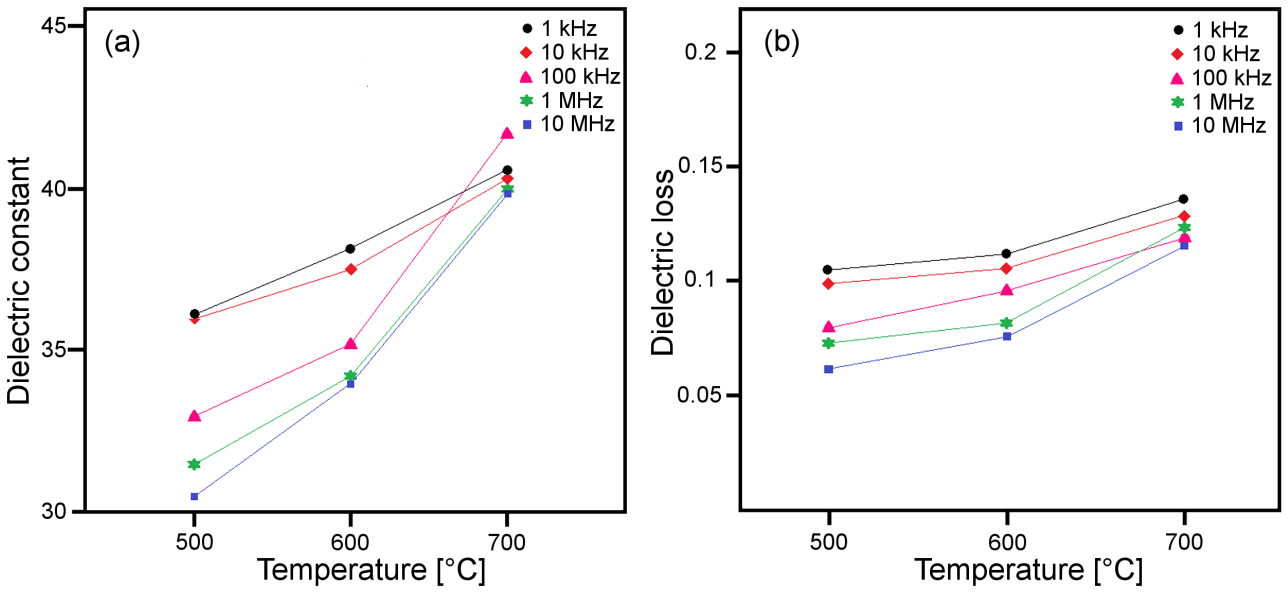

Figure 8. Variation of dielectric constant (a) and dielectric loss (b) of BSS2 thin film as a function of annealing temperature measured at different frequencies

lated defects [57,58]. Thus, in structures with fine grain size the pinning of the domain walls by grain boundaries makes the polarization process difficult to accomplish, and consequently increases dielectric loss [59]. Therefore, it could be expected that the BSS2 sample with finer grains compared to other bismuth silicate films shows higher dielectric loss.

The observed dispersion of both dielectric constant and dielectric loss at lower frequencies (Fig. 7) is consistent with Maxwell-Wagner interfacial polarization. The inhomogeneous dielectric and insulated structure of the composites induces space charges. In general, there is a characteristic relaxation time for charge transport and therefore both dielectric constant and dielectric loss depend on the applied frequency [60]. At higher frequency, the loss is small in all samples, which means that the prepared thin films could be used in practical applications such as oscillators.

The effect of annealing temperature on dielectric constant of the nanostructured BSS2 films at different frequencies of 1, 10, 100, 1000 kHz, and 10 MHz is presented in Fig. 8a. It could be found that, the dielectric constant of the BSS2 films increases with annealing temperature for all applied frequencies. With the increase in annealing temperature, the grain growth accelerates and as a result domain wall motion becomes easier. Thus, the observed change in dielectric properties obtained for the samples annealed at different temperatures could be explained by domain wall pining. Moreover, lower amount of secondary phase in the annealed sample at higher temperature results in higher dielectric constant [61]. Another reason for lower dielectric constant for the films annealed at 500 and 600 °C compared to 700 °C could be poor crystallinity at low temperatures [58].

The effect of annealing temperature on dielectric loss of the nanostructured BSS2 films at different frequencies of 1, 10, 100, 1000 kHz, and 10 MHz is presented in Fig. 8b. The dielectric loss increases with increase in annealing temperature and decreases with frequency. The increase of dielectric constant and dielectric loss with annealing temperature may be related to higher mobility of permanent dipoles which facilitate polarization [62]. Also, the observed change in dielectric properties for the synthesized thin films annealed at different temperatures may be explained by domain wall pining, which was determined by the degree of crystalline and the presence of secondary phases [61,63].

IV. Conclusions

Nanostructured BSO thin films with different Sr contents of 0, 1, 2, and 3 mol% were fabricated by sol-gel method and annealed at different temperatures up to 700 °C. SEM observations showed that the synthesized films were smooth and dense containing the equiaxed grains with the mean size of about 30–35 nm. The dielectric properties measurements indicated that the room temperature relative dielectric constant and dielectric loss of the samples decreased with increasing applied frequency and increased with increasing annealing temperature. The dielectric constant and dielectric loss decreased simultaneously with Sr addition, and reached the minimum for the sample containing 2 mol% Sr. We believe that it could be related to the crystal structure and formation of secondary phases.

References

1. N. Setter, D. Damjanovic, L. Eng, G. Fox, S. Gevorgian, S. Hong, A. Kingon, H. Kohlstedt, N.Y. Park, G.B. Stephenson, I. Stolitchnov, A.K. Taganstev, D.V. Taylor, T. Yamada, S. Streiffer, "Ferroelectric thin films: Review of materials, properties, and applications", *J. Appl. Phys.*, **100** (2006) 051606.

2. H. Ishiwara, "Ferroelectrics random access memories", *J. Nanosci. Nanotechnol.*, **12** (2012) 7619–7627.
3. Ju.H. Krieger, "Principle operation of 3-D memory device based on piezoacousto properties of ferroelectric films", pp. 3-18 in *Ferroelectrics*, Ed. I. Coondoo, InTech Open, 2010.
4. D. Seol, H. Taniguchi, J.-Yeol Hwang, M. Itoh, H. Shin, S.W. Kim, Y. Kim, "Strong anisotropy of ferroelectricity in lead-free bismuth silicate", *Nanoscale*, **7** [27] (2015) 11561–11565.
5. V.I. Burkov, Y.F. Kargin, V.V. Volkov, N.Y. Zubovich, "Spectroscopic and chirooptical properties of doped sillenite crystals. I. absorption and circular-dichroism spectra of $Bi_{12}SiO_{20}$ and $Bi_{12}TiO_{20}$ crystals doped with phosphorus and vanadium", *Neorg. Mater.*, **30** [8] (1994) 1078–1082.
6. Q.Q. Tian, X.F. Wang, C.L. Yu, H.T. Jiang, Z.G. Zhang, Y. Wang, S.B. Lin, "Domain structure and defects of highly ordered $Bi_4Si_3O_{12}$ micro-crystals", *Sci. China, Ser. E*, **52** [8] (2009) 2295–2301.
7. S.S. Slavov, M.Z. Krapchanska, E.P. Kashchieva, S.B. Parvanov, Y.B. Dimitriev, "Dielectric properties of bismuth titanate ceramics containing SiO_2 and Nd_2O_3 as additives", *Process. Appl. Ceram.*, **6** [3] (2012) 117–122.
8. B. Yang, J. Xu, Y. Zhang, Y. Chu, M. Wang, Y. Wen, "A yellow emitting phosphor Dy:$Bi_4Si_3O_{12}$ crystal for LED application", *Mater. Lett.*, **135** (2014) 176–179.
9. B. Aurivillius, "Mixed bismuth oxides with layer lattices. 2. Structure of $Bi_4Ti_3O_{12}$", *Arkiv for Kemi*, **1** [6] (1950) 499–512.
10. E.O. Klebansky, A.Y. Kudzin, V.M. Pasalskii, S.N. Plyaka, L.Y. Sadovskaya, G.K. Sokolyanskii, "Thin sol-gel bismuth silicate films", *Phys. Solid State*, **41** [6] (1999) 913–915.
11. J. Harjuoja, S. Vayrynen, M. Putkonen, L. Niinisto, E. Rauhala, "Crystallization of bismuth titanate and bismuth silicate grown as thin films by atomic layer deposition", *J. Cryst. Growth*, **286** [2] (2006) 376–383.
12. A. Golubovic, S. Nikolic, R. Gajic, S. Djuric, A. Valcic, "The growth and optical properties of $Bi_{12}SiO_{20}$ single crystals", *J. Serb. Chem. Soc.*, **67** [4] (2002) 279–289.
13. Q. Han, J. Zhang, X. Wang, J. Zhu, "Preparing $Bi_{12}SiO_{20}$ crystals at low temperature through nontopotactic solid-state transformation and improving its photocatalytic activity by etching", *J. Mater. Chem. A*, **3** [14] (2015) 7413–7421.
14. T.V. Panchenko, S.Y. Kopylova, "Photochromic properties of the doped $Bi_{12}SiO_{20}$ crystals", *Ferroelectrics*, **322** [1] (2005) 69–74.
15. C.H. Hervoches, P. Lightfoot, "Cation disorder in three-layer Aurivillius phases: Structural studies of $Bi_{2-x}Sr_{2+x}Ti_{1-x}Nb_{2+x}O_{12}$ ($0 < x < 0.8$) and $Bi_{4-x}La_xTi_3O_{12}$ (x = 1 and 2)", *J. Solid State Chem.*, **153** [1] (2000) 66–73.
16. J.D. Bobić, M.M. Vijatović Petrović, B.D. Stojanović, "Aurivillius $BaBi_4Ti_4O_{15}$ based compounds: Structure, synthesis and properties", *Process. Appl. Ceram.*, **7** [3] (2013) 97–110.
17. E.C. Aguiar, A.Z. Simões, F. Moura, M. Cilense, E. Longo, J.A. Varela, "Piezoresponse force microscopy behaviour of $Bi_4Ti_3O_{12}$ ceramics with various excess bismuth", *Process. Appl. Ceram.*, **5** [1] (2011) 1–11.
18. J.D. Bobić, M.M. Vijatović, T. Rojac, B.D. Stojanović, "Characterization and properties of barium bismuth titanate", *Process. Appl. Ceram.*, **3** [1-2] (2009) 9–12.
19. A. Fouskova, L.E. Cross, "Dielectric properties of bismuth titanate", *J. Appl. Phys.*, **41** [7] (1970) 2834–2838.
20. T. Jardiel, A.C. Caballero, M. Villegas, "Aurivillius ceramics: $Bi_4Ti_3O_{12}$-based piezoelectrics", *J. Ceram. Soc. Jpn.*, **116** [4] (2008) 511–518.
21. E.K. Choi, S.S. Kim, J.K. Kim, J.C. Bae, W.-J. Kim, Y.-I. Lee, T.K. Song, "Effects of donor ion doping on the orientation and ferroelectric properties of bismuth titanate thin films", *Jpn. J. Appl. Phys.*, **43** [1] (2004) 237–241.
22. U. Chon, H.M. Jang, M.G. Kim, C.H. Chang, "Layered perovskites with giant spontaneous polarizations for nonvolatile memories", *Phys. Rev. Lett.*, **89** [8] (2002) 087601.
23. U. Chon, J.S. Shim, H.M. Jang, "Ferroelectric properties and crystal structure of praseodymium-modified bismuth titanate", *J. Appl. Phys.*, **93** [8] (2003) 4769–4775.
24. M. Chen, Z.L. Liu, Y. Wang, C.C. Wang, X.S. Yang, K.L. Yao, "Ferroelectric properties and microstructures of Sm-doped $Bi_4Ti_3O_{12}$ ceramics", *Physica B: Condensed Matter*, **352** [1-4] (2004) 61–65.
25. T. Watanabe, H. Funakubo, M. Osada, H. Uchida, I. Okada, "The effects of neodymium content and site occupancy on spontaneous polarization of epitaxial $(Bi_{4-x}Nd_x)Ti_3O_{12}$ films", *J. Appl. Phys.*, **98** [2] (2005) 024110.
26. C.Y. Yau, R. Palan, K. Tran, R.C. Buchanan, "Mechanism of polarization enhancement in La-doped $Bi_4Ti_3O_{12}$ films", *Appl. Phys. Lett.*, **86** [3] (2005) 032907.
27. A.Z. Simoes, C. Quinelato, A. Ries, B.D. Stojanovic, E. Longo, J.A. Varela, "Preparation of lanthanum doped $Bi_4Ti_3O_{12}$ ceramics by the polymeric precursor method", *Mater. Chem. Phys.*, **98** [2-3] (2006) 481–485.
28. A.F. Lima, S.O. Souza, M.V. Lalić, "Electronic structure and optical absorption of the $Bi_4Ge_3O_{12}$ and the $Bi_4Si_3O_{12}$ scintillators in ultraviolet region: An ab initio study", *J. Appl. Phys.*, **106** [1] (2009) 013715.
29. H. Xie, F. Li, C. Chen, H. Xi, X. Wang, X. Zhu, "Sol-gel preparation and characterization of $Bi_4(Si_{1-x}Ge_x)_3O_{12}$ solid solutions", *J. Sol-Gel Sci. Technol.*, **72** [1] (2014) 37–42.
30. Y.N. Nagao, Y. Mimura, "Epitaxial growth of $Bi_{12}SiO_{20}$ films by chemical vapor deposition", *Jpn. J. Appl. Phys.*, **24** [12] (1985) 954–955.
31. A. Veber, S. Kunej, D. Suvorov, "Synthesis and microstructural characterization of $Bi_{12}SiO_{20}$ (BSO) thin films produced by the sol-gel process", *Ceram. Int.*, **36** [1] (2010) 245–250.
32. J.C. Alonso, R. Diamant, E.H. Poniatowski, M.F. Guasti, G. Munoz, I. Camarillo, M. Jouanne, J.F. Morhange, "Raman characterization of $Bi_{12}SiO_{20}$ thin films obtained by pulsed laser deposition", *Appl. Surf. Sci.*, **109-110** (1997) 359–361.
33. T. Okada, F. Yahiro, H. Uetsohara, Y. Nakata, M. Maeda, S. Higuchi, "Deposition of highly oriented $Bi_{12}SiO_{20}$ thin films on Y-stabilized zirconia and SiO_2 by pulsed-laser deposition", *Appl. Phys. A*, **69** [1] (1999) S723–S726.
34. N. Thanabodeekij, E. Gulari, S. Wongkasemjit; "$Bi_{12}TiO_{20}$ synthesized directly from bismuth (III) nitrate pentahydrate and titanium glycolate and its activity", *Powder Technol.*, **160** [3] (2005) 203–208.
35. G.J. Owens, R.K. Singh, F. Foroutan, M. Alqaysi, C.-Min Han, C. Mahapatra, H.-Won Kim, J.C. Knowles, "Sol-gel based materials for biomedical applications", *Prog. Mater. Sci.*, **77** (2016) 1–79.

36. C.J. Brinker, G.C. Frye, A.J. Hurd, C.S. Ashley, "Fundamentals of sol-gel dip coating", *Thin Solid Films*, **201** [1] (1991) 97–108.
37. X. Zhu, J. Xie, D. Lin, Z. Guo, J. Xu, Y. Shi, F. Lei, Y. Wang, "Synthesis of BSO ($Bi_4Si_3O_{12}$) scintillation thin film by sol-gel method", *J. Alloys Compd.*, **582** (2014) 33–36.
38. A. Sadeghzadeh Attar, M. Sasani Ghamsari, F. Hajiesmaeilbaigi, Sh. Mirdamadi, "Modifier ligands effects on the synthesized TiO_2 nanocrystals", *J. Mater. Sci.*, **43** [5] (2008) 1723–1729.
39. X.J. Dai, S. L. Yong, S.Y. Fu, W.Q. Chen, Y. Lu, "Facile hydrothermal synthesis of 3D hierarchical Bi_2SiO_5 nanoflowers and their luminescent properties", *Solid State Sci.*, **12** [4] (2010) 637–642.
40. H. Zhang, S. Jiang, K. Kajiyoshi, "Preparation and characterization of sol-gel derived sodium-potassium bismuth titanate powders and thick films deposited by screen printing", *J. Alloys Compd.*, **495** [1] (2010) 173–180.
41. P. Somasundaram, *Encyclopedia of surface & colloid science*, 2nd Ed., Taylor & Francis group, CRC Press, 2006.
42. H. Xie, C. Jia, Y. Jiang, X. Wang, "Synthesis of $Bi_4Si_3O_{12}$ powders by a sol-gel method", *Mater. Chem. Phys.*, **133** [2-3] (2012) 1003–1005.
43. V. Somani, S.J. Kalita, "Synthesis and characterization of nanocrystalline barium strontium titanate powder via sol-gel processing", *J. Electroceram.*, **18** [1-2] (2007) 57–65.
44. A.A. Vodyankin, I.P. Ushakov, Y.A. Belik, O.V. Vodyankina, "Synthesis and photocatalytic properties of materials based on bismuth silicates", *Kinet. Catal.*, **58** [5] (2017) 593–600.
45. H.W. Guo, X.F. Wang, D.N. Gao, "A novel method for preparation of pure Bi_2SiO_5 crystals", *Mater. Lett.*, **67** [1] (2012) 280–282.
46. Joint Committee on Powder Diffraction Standard (JCPDS), International Center for Diffraction Data, Swarthmore, PA, 1996.
47. M. Villegas, T. Jardiel, A.C. Caballero, J.F. Fernandez, "Electrical properties of bismuth titanate based ceramics with secondary phases", *J. Electroceram.*, **13** [1-3] (2004) 543–548.
48. S. Hajijafari-Bidgoli, A. Sadeghzadeh-Attar, M.R. Bafandeh, "Structural and optical properties of Sr-modified bismuth silicate nanostructured films synthesized by sol gel method", *J. Nanostruct.*, **7** [4] (2017) 258–265.
49. B.D. Cullity, *Elements of X-ray Diffraction*, Addison Wesley pub., Menlo Park, CA, USA, 1978.
50. L. Gao, J. Zhai, X. Yao, "The influence of Co doping on the dielectric, ferroelectric and ferromagnetic properties of $Ba_{0.70}Sr_{0.30}TiO_3$ thin films", *Appl. Sur. Sci.*, **255** [8] (2009) 4521–4525.
51. R. Chaim, M. Levin, A. Shlayer, C. Estournes, "Sintering and densification of nanocrystalline ceramic oxide powders: A review", *Adv. Appl. Ceram.*, **107** [3] (2008) 159–169.
52. P. Mythili, T. Kanagasekaran, G. Bhagavannarayana, R. Gopalakrishnan, "Studies on crystal growth, optical and electrical characterization of pure and Dy-doped bismuth silicate single crystals", *J. Cryst. Growth*, **338** [1] (2012) 222–227.
53. A.Z. Simões, A. Ries, F. Moura, C.S. Riccardi, E. Longo, J.A. Varela, "Influence of the solution pH on the morphological, structural and electrical properties of $Bi_{3.50}La_{0.50}Ti_3O_{12}$ thin films obtained by the polymeric precursor method", *Mater. Lett.*, **59** [22] (2005) 2759–2764.
54. A. Sadeghzadeh Attar, E. Salehi Sichani, S. Sharafi, "Structural and dielectric properties of Bi-doped barium strontium titanate nanopowders synthesized by sol-gel method", *J. Mater. Res. Technol.*, **6** [2] (2017) 108–115.
55. L.M. Nunes, E. Antonelli, M.I.B. Bernardi, T.O. Oladeinde, J.A.S. Caceres, J.-C. M'Peko, "How grain boundaries modify the high-temperature dielectric response of ferroelectric electroceramics like $BaTiO_3$?", *Mater. Res. Bull.*, **46** [1] (2011) 136–139.
56. V.R. Mudinepalli, L. Feng, W.-C. Lin, B.S. Murty, "Effect of grain size on dielectric and ferroelectric properties of nanostructured $Ba_{0.8}Sr_{0.2}TiO_3$ ceramics", *J. Adv. Ceram.*, **4** [1] (2015) 46–53.
57. V.M. Ferreira, J.L. Baptista, "Preparation and microwave dielectric properties of pure and doped magnesium titanate ceramics", *Mater. Res. Bull.*, **29** [10] (1994) 1017–1023.
58. H. Wang, M.F. Ren, "Low temperature synthesis and ferroelectric properties of La substituted $Bi_4Ti_3O_{12}$ thin films by sol-gel", *Mater. Sci. Eng. B*, **122** [3] (2005) 201–205.
59. A.Z. Simoes, G.C.C. da Costa, M.A. Ramirez, J.A. Varela, E. Longo, "Effect of the excess of bismuth on the morphology and properties of the $BaBi_2Ta_2O_9$ ceramics", *Mater. Lett.*, **59** [6] (2005) 656–661.
60. Y. Guo, S. Feng, N. Wang, B. Wang, M. Gu, "$Bi_4Ti_3O_{12}$-$(Ni_{0.5}Zn_{0.5})Fe_2O_4$ dielectric-ferromagnetic ceramic composites synthesized with nanopowders", *Mater. Chem. Phys.*, **124** [1] (2010) 184–187.
61. B.-Cheng Sun, H. Wang, J.-Wen Xu, L. Yang, S.-Ju Zhou, Y.-Pei Zhang, Z.-Da Li, "Effect of annealing temperature on resistance switching and dielectric characteristics of $Bi_4Ti_3O_{12}$ thin films", *Microelectron. Eng.*, **113** (2014) 1–4.
62. A.J. Moulson, J.M. Herbert, *Electroceramics: Materials, Properties, Applications*, 2nd Edition, John Wiley & Sons, New York, 2003.
63. F. Suhua, C. Wen, Z. Fengqing, H. Guangda, "Effects of excess bismuth on structure and properties of $SrBi_4Ti_4O_{15}$ ceramics", *J. Rare Earth*, **25** [2] (2007) 317–321.